Preliminary observations and simulation of Nocturnal variations of airglow temperature and emission rates at Pune (18.5^{O}N), India

S. Fadnavis[1], W. Feng[2,3], Gordon G. Shepherd[4], J.M.C. Plane[2], S. Sonbawne[1], Chaitri Roy[1], S. Dhomse[3], S.D. Ghude[1]

[1]Indian Institute of Tropical Meteorology, Pune, India.

[2]School of Chemistry, University of Leeds, Leeds, UK.

[3] National Centre for Atmospheric Science, School of Earth and Environment, University of Leeds, Leeds, UK.

[4]Centre for Research in Earth and Space Science, York University, Toronto, Canada.

Abstract

Preliminary observations of the nocturnal variations of the OH(6-2) and O2b(0-1) nighttime airglow in the mesosphere and lower thermosphere are investigated in the context of tidal influence for the tropical latitude station Pune (18.5^{O}N, 73.85^{O}E). This is the only tropical Spectral Airglow Temperature Imager (SATI) station where the tidal variations of mesosphere and lower thermosphere (MLT) temperature have been determined from ground based SATI observations. The SATI observations obtained since October 2012 reveal the influence of the migrating semidiurnal tides during solstice at this tropical station. There is variability in amplitude and phase obtained from SATI observations. In this paper, SATI observations on 10 Dec 2012 and 3March 2013 are compared with Whole Atmosphere Community Climate Model (WACCM) simulations. The amplitude of semidiurnal tides is ~25K/30K on 10 Dec 2012 during solstice for OH/O_2 temperature. During equinox SATI data indicates existence of semidiurnal tide also. The airglow observations are compared with simulations from the WACCM. The model underestimates the amplitude of the semi diurnal tide during equinox (1.6 K/2.7 K at 87 km/96 km) and solstice (~3.8 K/4.8K at 87 km/96 km) for these days. The reason may be related to dampening of tides in the model due to the effect of strong latitudinal

shear in zonal wind. The diurnal variation of airglow emission - which the model simulates well - is related to the vertical advection associated with the tides and downward mixing of atomic oxygen.

Key words: Spectral airglow, mesosphere, temperature, Whole Atmosphere Community Climate Model (WACCM).

1. **Introduction**

. It has been known for the last few decades that the most prominent motions in the mesosphere and lower thermosphere (MLT) are atmospheric tides which dominate the meridional wind field at low latitudes (Hays et al., 1994; Lieberman et al., 2007). The variability in the diurnal tide in the mesosphere and lower thermosphere is discussed by Hagan (1997). A brief description of tides is given below.

Atmospheric tides are an integral part of the general circulation and play an important role in coupling between the lower and upper atmosphere (e.g. Hagan, 2000; Zeng et al., 2008). Tides that propagate into the MLT affect the large-scale dynamics, chemistry, and energetics of this region. They may transport momentum and energy upward from the source regions (the troposphere and stratosphere), modulate the fluxes of gravity waves (Manson et al., 1998), and dissipate in the MLT region (e.g. Forbes et al. 1993; Miyahara et al. 1993).

Tides also play a major role in the diurnal cycle of chemical species and transport in the MLT region (Ward et al. 1999; Marsh and Russell 2000; Zhang et al. 2001) and therefore influence chemical heating/cooling (Smith et al. 2003). Airglow observations also show strong seasonal variation in the amplitude of diurnal and semidiurnal tides (López-González et al., 2005). The tidal variability is so dominant that the seasonal cycle in the nighttime emission depends very strongly on the local time of the analysis (Marsh et al ., 2013).

Ground-based measurements have helped to delineate the characteristic tidal motions of the middle atmospheric temperature and winds (e.g. Shepherd et al., 1998; Zhou et al., 2000; Akmaev, 2001; Yuan et al., 2008a,b; Gurubaran et al., 2009; Jaya Prakash Raju et al., 2010; Hibbins et al., 2011). Studies pertaining to tropical regions are based on satellite observations (McLandress et al., 1996; McLandress, 2002, Lieberman et al., 2007; Zeng et al., 2008; Liu et al., 2008), radar/lidar observations (Manson et al., 2003; Gurubaran et al., 2005; 2009; Pant et al., 2004; 2007) and airglow rotational temperatures (e.g. Taori et al. 2005, 2007, 2010, 2012; Taori and Taylor 2006; Guharay et al. 2009; Ghodpage et al. 2015; Kishore Kumar et al., 2008; 2014).

The main advantage of ground-based observations at a specific geographical location is that they provide continuous long-term measurements at very high temporal resolution and at all local times on a given night, but optical measurements such as lidar or airglow provide data only during nighttime hours, insufficient to separate the diurnal and semidiurnal tides. In contrast, satellite measurements can provide a near-global picture over 24 hours of local time, but their measurements at a given latitude on a single day are for just two local times, one for the daytime side of the orbit and one for the night time; which changes from day to day.

Tidal influences on the diurnal emission rate of $O(^1S)$ were the first strong indication that dynamics are responsible for variations in the emission rate (Shepherd et al., 1995, 2012).

Details of their diurnal and seasonal variation are still under investigation (McLandress, 2002; López-González et al., 2004, 2007; Liu et al., 2008). These observations also exhibit a strong diurnal tide at the equator. The meridional and zonal wind components attain their maximum values at equinox, while the solstitial minima are smaller by nearly a factor of 2 around 20^{O} N and 20^{O} S. Vertical advection of atomic oxygen associated with the tides has been proposed to be the primary mechanism for the diurnal variation of the $O(^1S)$ airglow at the equator (Angelats i Coll and Forbes, 1998; Ward, 1999) but confirmation with a ground-based instrument in the tropics has so far been lacking. Atomic oxygen plays an important role in the production of the OH and O_2 bands (McDade, and Llewellyn, 1986). TIME-GCM simulations also suggest that the advection of the mean circulation is responsible for the transport of atomic oxygen (Liu and Roble, 2004).

Temperature variations in the migrating tides have been less well studied. Mukhtarov et al. (2009) employed satellite data provided by the Sounding of the Atmosphere using Broadband Emission Radiometry (SABER) instrument on the Thermosphere Ionosphere Mesosphere Energetics and Dynamics (TIMED) satellite to present the global characteristics of the diurnal migrating tide. This study showed strong diurnal tides from 15° S to 15° N latitude, showing a seasonal cycle with maxima at equinoxes. Somewhat weaker amplitudes, with a semiannual variation, were observed poleward of about 25° in latitude. In between the equatorial and mid-latitudes there was a narrow “slot” in which the diurnal temperature amplitudes are very small.

The Spectral Airglow Temperature Imager (SATI), described by Sargoytchev et al. (2004) is able to determine the airglow emission rate and rotational temperatures from the OH Meinel (6,2) and O_2 Atm (0,1) bands. The performance at a higher latitude station has been well demonstrated by López-González et al., (2005; 2007). In this paper, preliminary observations of airglow measurements at the tropical station Pune (18.5ºN, 73.8ºE) from ground-based SATI observations are reported for the first time. The new Pune results are compared against simulations from a 3D Chemistry Climate Model (CCM), the Whole Atmosphere Community Climate Model (WACCM) (Chang et al., 2012; Feng et al., 2015). There are only a few ground-based studies of the variation of airglow intensity over the Indian region (Gogawale and Tillu, 1983; Ranade et al., 1988; Ghodpage et al., 2012), and they did not report temperature measurements.

The paper is structured as follows: section two describes the airglow measurements and WACCM model run. Section three gives details of the observed diurnal variations of temperature and emission rates during equinox and solstice. The influence of diurnal tides as observed in airglow temperature and emission rate, and WACCM results on the MLT temperature, are presented in section 3. Model and observed tidal characteristics are given in section 4. Key results including the correlation between airglow temperature and emission rates as well as vertical advection associated with tides and downward mixing of atomic oxygen are discussed in Section 5 and conclusion are made in section 6.

2. Airglow Data and WACCM experimental setup

2.1 The Spectral Airglow Temperature Imager (SATI)

The Spectral Airglow Temperature Imager (SATI) is a spatial and spectral scanning Fabry-Perot spectrometer, comprising a conical mirror, Fresnel lens, a CCD detector and narrow-band interference filters centered at (1) 867.6 nm (O_2 atmospheric (0-1) band) and (2) 836.8 mn (OH Meinel (6-2) band) (López-González et al., 2004). Its field of view is an annulus of

30^o average radius and 7.1^o angular width centered on the zenith. It measures the column emission rate for several rotational lines and the rotational temperature is inferred from their ratios (Sargoytchev et al. 2004). The images obtained correspond to a ring of observation on the sky observed. The radial distribution of the image provides information on the spectral distribution while the azimuthal sectors correspond to different azimuths on the sky. In this study the images are analyzed as a whole (obtained from whole sky ring) to obtain an average of the rotational temperature and emission rate of the airglow. The exposure time is 120 seconds and time resolution is 4 minutes for the OH and O_2 airglow layers. The instrument error for both the OH and O_2 relative temperature is ~1.7 K, and ~2% for emission rates. Further details of the SATI instrument and image reduction method are documented by López-González al. (2005) and Sargoytchev et al. (2004). The SATI was built by CRESS (the Centre for Research in Earth and Space Science at York University, Toronto). The SATI Airglow observations at Pune used in this study is for 14 individual nights during the period October 2012- December 2014, eight nights of data for equinox conditions and six nights of data for solstice conditions.

In this paper, the influence of the sun-synchronous and migrating diurnal tides at the tropical station Pune (18.5°N, 73.8°E) from ground-based SATI observed temperature and OH and O_2 airglow intensity, are reported for the first time. The results are compared against simulations from a 3D Chemistry Climate Model (CCM), the Whole Atmosphere Community Climate Model (WACCM) (details are given in the next section 2.2). The model simulations are used to study the dynamical changes in temperature, airglow intensity, and the atomic oxygen flux. Western Ghats around Pune is a gateway for monsoon convection. This hilly region may be a source of strong gravity/mountain waves and may impact mesospheric waves.

In the past, the High Resolution Dynamics Limb Sounder (HIRDLS) on the Aura satellite which measured temperature profiles of the atmosphere, has shown propagation of mountain waves into the mesosphere (Joan, 2008).Due to the lack of a longer time series, this study is focused on the equinox and solstice periods.

2.2 **Whole Atmosphere Community Climate model (WACCM) experimental setup**

We employ WACCM (version 4) ((Marsh et al., 2013), a “high-top” coupled chemistry-climate model with an upper boundary at 6.0×10^{-6} hPa (~140 km) to understand dynamical processes in the mesosphere and lower thermosphere (MLT) region. WACCM reproduces diurnal and semidiurnal tide in the MLT (Chang et al., 2012, Feng et al., 2015). We have used the specified dynamics version nudged (forced) with the Goddard Earth Observing System 5 (GEOS-5) meteorological data set (Feng et al., 2013; Plane 2014). A nudging coefficient value (0.01) was used when assimilating the GEOS-5 analysis into WACCM, so that 1% of the meteorological conditions were combined with WACCM fields below 60 km at every model dynamics time step. Above 60 km the model was free running with a horizontal resolution of $1.9° \times 2.5°$ and ~3.5 km vertical resolution in the MLT. The Prandtl number is set to 4. We sampled the model output every 30 min from January 2012 until the end of December 2013.

The OH and O_2 volume emission rates were estimated by integrating the product of $k_{H+O3}[H][O_3]$, and $k_{O+O}[O]^2[M]$ (Chamberlain, 1961), where the temperature-dependent rate coefficients are taken from Sander et al. (2006). Because this approach does not include quenching of the excited states, WACCM emission rates are scaled to best match the SATI observations. Because the daytime emission processes are different they are not considered here.

Furthermore, the emissions occur over several vibrational bands, whereas the narrow-band SATI measures emission in a single band e.g. the (6,2) Meinel band for OH.

3. The variation of airglow temperature and emission rate.

Figures 1a – d exhibit variations of OH temperature and emission rate for all the days of observation during solstice and equinox. There is a significant variation in peak temperatures. On few nights, for example 10 December 2012 and 14 December 2012 there is significant variation in nocturnal temperature while variability is weak on 10 December 2014 and 23 Dec 2014. On some nights there is peak in temperature 2 hours before local midnight. The emission rates vary and the pre-midnight peak is not always evident. The measurement of emission rate is subject to light cloud which may not otherwise be recognized, but the temperature, which depends on the ratio of two emission rates is not affected. During the equinox, temperature and emission rates generally peak before midnight, but for a few nights higher emission values are observed after midnight. As noted earlier the emission rates are significantly lower at equinox than at solstice.

3.1 The variation of airglow temperature and emission rate during solstice.

Figures 2 (a) and (b) illustrate the variation of the OH temperature and emission rates on 10 December 2012 and the respective values are shown for O_2 in Figures 2(c) and 2(d). These observations are also compared with WACCM simulations for the altitudes of 87 km for OH and 95 km for O_2. A simulated sinusoidal waveform applied to the SATI data (red color) provides a comparison with a semidiurnal variation. This variation is consistent with the presence of a semidiurnal tide in the SATI OH and O2 temperature and emission rate although not definitive because of the short local time scale. The WACCM temperatures for the OH and O_2 altitudes have ranges of 12 K peak to valley and 20 K respectively on 10 December 2012. While the WACCM temperatures for the OH altitude appear to have a diurnal component superimposed on the semidiurnal those for the O_2 altitude appear purely semidiurnal so the characteristics at the two altitudes are somewhat different. The maximum of tide in the SATI temperature in OH measurements is similar to WACCM (figure 2(a)), while SATI temperatures are smaller than WACCM (by more than 20K) in the minimum. But, on average, WACCM temperatures are warmer by about 15K. The SATI observed temperature in O2 measurements is similar to WACCM (figure 2(c)) in the minimum of the detected tide while maximum SATI temperatures are larger than WACCM by 40K. Now SATI temperatures are warmer on average by about 15K. The mean SATI temperature observed in OH measurements is colder (underestimated), while the mean SATI temperature observed in O2 measurements is warmer (overestimated) than the mean temperature simulated by WACCM. The observed SATI temperatures are roughly 30 K higher for O_2 than for OH, suggesting that the O_2 layer at 94 km is above the mesopause. Figures 2(a) and 2(c) show that the amplitude of the tide observed on 10 December 2012 is larger than the amplitude of the nocturnal variation simulated by WACCM at both (OH and O_2) altitudes. Thus mean amplitude simulated by WACCM seems to be underestimated respect to the nocturnal variation observed by SATI on 10 December 2012. The reason for this may be related to damping of tidal amplitude in the WACCM simulations (Feng et al., 2013). The conversion of WACCM atmospheric pressure to altitude is also a possible source of difference.

Both the temperature and OH emission rate from SATI and WACCM show a pronounced maximum about ~1.5 hour before local midnight. Figure 2 (c) shows that the O_2 temperature peaks ~3 hours before midnight. Ghodpage et al. (2012) observed a maximum in the higher altitude OI 557.7 nm intensity 3-4 hours before midnight during equinox at the Indian station Kolhapur (16.8^{O}N, 74.2^{O}E). Whereas the airglow measurements (OH and O_2 emission rates and temperature) at the mid-latitude station at the Sierra Nevada Observatory (37.06◦ N, 3.38◦ W) show a maximum 2 hours after midnight during winter solstice (López-González et al., 2005). A comparison of figures 2(a) and 2(c) shows that the peak in O_2 temperature around 95 km occurs about 1 to 1.5 hours before the peak in OH temperature (around 87 km), which is evidence of downward phase propagation of an upward-propagating semi-diurnal tidal wave.. Different values of phase delay between OH and O2 temperature and intensity at different latitude and season conditions have been reported in the past (Hernandez et al.,1995; Vargas et al., 2007; Taori et al., 2007; Takahashi et al., 2011).

3.2 The variation of airglow temperature and emission rate during equinox.

During equinox (March-April) Pune experiences frequent thunderstorms which last a few hours and weather becomes clear thereafter. Thunderstorm activity therefore causes the airglow observations to be intermittent. Hence, the SATI OH emission rates and temperature have been averaged for half an hour around each time shown in Figure 3. The data on O_2 emission rates and temperature is sparse (2-5 nights per month) during this period. Figures 3(a) and (b) illustrate the variation of the averaged OH temperature and emission rates on 3 March 2013. Again, the WACCM simulated temperature at 87 km and OH emission rates are included for comparison, showing that the mean temperature in the model is colder than the SATI observations on 3 March 2013. The red line is a simulated sinusoidal curve applied to the SATI observations, consistent with the existence of a semidiurnal tide over this short local time range. As discussed earlier it is not possible to separate diurnal and semidiurnal components from observations during night time hours only (Crary and Forbes, 1983). WACCM simulations show during this equinox the existence of a dominant migrating diurnal tide. The amplitude of the diurnal is stronger than the semidiurnal tide (discussed in section 5). On 3 March 2013, the minimum and maximum in SATI temperature is warmer than WACCM. Figures 2 and 3 show that the shape of the nocturnal variation of temperature is similar on 10 December 2012 and 3 March 2013. The observed maximum temperature is ~280 K on 3 March 2013 and ~220 K on 10 December 2012. The observed maximum temperature on 3 March 2013 may be anomalous or it may be due to seasonal variation. The plots of hourly variation in SABER temperature also show temperature reaching up to ~250K on few days and ~200K on other days at a mid-latitude station (37.06^{O} N, 3.38^{O}W) (López-González et al.,2007, figure 6 therein).

4. Model and observed tidal characteristics

The tropical MLT region is dominated by the semidiurnal/diurnal migrating tides (McLandress et al., 1996). In order to understand the tidal influence on MLT temperature, we analyze anomalies in temperature as obtained from WACCM simulations during equinox and solstice. Figures 4(a) and (b) shows anomalies in WACCM temperature between 65 km and 120 km, on 10 December 2012 and 3 March 2013, as representative of solstice and equinox, respectively. The anomalies are obtained by subtracting the respective monthly mean temperatures for each altitude. The downward propagating alternate positive and negative temperature anomalies are seen during equinox and solstice. From the temporal variations at 87 or 95 km, one can see in figure 4 that diurnal tides prevail on 3 March 2013 (equinox), and semidiurnal tide on 10 December 2012 (solstice) and the distinction is even clearer at higher altitudes. A Fast Fourier Transform (FFT) analysis of the temperature time series from the WACCM simulations (at 87km and 95km) also reveals strong diurnal tides during equinox, and semi-diurnal during solstice (discussed in later in this section, Figure 5). A simulated sinusoidal curve fit on SATI OH temperature on 10 Dec 2012 shows amplitude of semidiurnal tide as 25K while at 87 km, WACCM shows mean amplitude of semidiurnal tide as 3.8K and diurnal tides as 1.8 K. The amplitude in SATI temperature is obtained from a curve fitted for about 8 hours, while the amplitude in WACCM temperature is estimated from an interval of 18 hours. As shown in Figure 4 the tidal patterns are complex, changing from day to day and even during one day and suggesting the presence of additional components. The derived amplitude for the WACCM temperature is averaged over solstice/equinox while that from SATI is for single day. This may be a reason why the retrieved amplitudes in WACCM are so small compared those of SATI on individual days. During March WACCM simulations show stronger diurnal amplitudes than do the semidiurnal tide. SATI OH temperature on 3 March also indicates a semidiurnal tide amplitude of ~38K. The nocturnal variation of ROSE model simulated temperature is ~40K at the equator (Marsh et al., 2006). As we have already seen in the comparison with SATI data, the variability in the amplitude for this day is larger than the obtained by WACCM. Amplitude of the semidiurnal tide larger than WACCM has been reported in the past by Smith, (2012), Liu et al., (2013), Feng (2015). Zhu et al. (1999) suggested that tides may be strongly damped in the model due to the strong effect of zonal mean winds. McLandress et al. (2002) reported that strong latitudinal shear in the zonal wind is responsible for weakening of the tide in the model. HAMMONIA model simulations by Beig et al. (2012) reported amplitudes of diurnal tides ~20 K in the upper mesosphere. From

Global Scale Wave Model and SABER measurements, Zhang et al. (2010) reported amplitudes of the diurnal tides at 95km or 110 km ~20 K, and ~6 K for the semidiurnal tide.

Figure 5(a) - (d) depict the vertical variation of the amplitude and phase of the diurnal and semidiurnal tides, estimated from the WACCM night-time temperatures during December and March (average for 2012 and 2013) as representative of solstice and equinox, respectively. Figure 5(a) shows that during solstice the semidiurnal tide dominates the MLT region at low latitudes, with amplitude nearly double that of the diurnal tides (except between 82 - 85 km). During equinox the diurnal tide dominates with amplitude almost double that of the semidiurnal tide (Figure 5 (c)). Figure 5(d) shows that there is phase reversal at about ~84 km, for the semidiurnal tide, and at about ~88 km, for the diurnal tide. SABER results and GSWM model show semidiurnal steep phase change at ~90-92 km at Arecibo, Puerto Rico (18.3°N, 66.8°W) and Maui, Hawaii (20.7°N, 156.3°W) stations, suggesting presence of a dominant non-migrating tide of long wavelength (Friedman et al., 2009). A number of papers in the past have reported similar results at tropical sites (Hecht, et al., 1993; Schubert et al.,1999; Walterscheid et al., 2000; Friedman, and Chu, 2007).

5. Correlations between temperature and OH emission rate

Figures 6 (a), (b) and (c) illustrate correlations between temperature and emission rates for OH and O_2 airglow on 10 December 2012 and 3 March 2013, measured by SATI. A significant positive correlation with a correlation coefficient $R > 0.72$ is observed on these nights. A similar positive correlation ($R > 0.76$) is also obtained between the WACCM temperature at 87 km/95 km and WACCM OH/O_2 emission rates (Figures 6 ((d), (e) and (f)). From SATI observations and model simulations, Cho and Shepherd, (2006) also reported a positive correlation between temperature and emission rates for OH and O_2 at Resolute Bay (74.8^{o}N). Takahashi et al (2004) and Espy et al., (2007) also reported similar results at Shigaraki (34.9^{O}N, 136.1^{O}E) and Stockholm (59.5°N, 18.2°E) respectively. The correlation is consistent with the presence of vertical motions (Takahashi et al., 2004; Cho and Shepherd, 2006; Shepherd et al. 2012, Espy et al., 2007). The analysis of correlation between temperature and emission rate indicates that the correlation coefficient is different for each day but the correlation is positive. This is likely an indication of day-to-changes in the vertical profiles of atomic oxygen concentration and temperature. The model simulations by Cho and Shepherd (2006) suggested that at higher latitude (74.8^{o}N), the peak altitude of emission is related to the emission rate, larger emission rates corresponds to lower peak altitude. Thus observed positive correlation between temperature and emission rate indicates that dominance of dynamics over chemistry.

We now estimate the upward/downward fluxes of atomic oxygen 1/(m^2 s) due to vertical advection, using WACCM data. The fluxes (f) are obtained from the product of the vertical wind velocity (w) and the atomic oxygen number density (N) i.e. f = w*N (Liu et al., 2008). Figures 7(a) and (b) show the calculated atomic oxygen fluxes corresponding to vertical advection. The variation of the flux has a semidiurnal pattern on 10 December 2012, and a mainly diurnal pattern on 3 March 2013. It can be seen that the amplitude of the atomic oxygen flux on 10 December 2012 is consistent with the variation of the SATI observed O_2 temperature and emission rates, reflecting the dominant influence of the semidiurnal tide. For 3 March 2013 the period of about 16 hours suggests the presence of a semidiurnal component in addition to the diurnal.

6. Conclusions

The airglow temperature and emission rates (for 14 nights) were measured using a ground-based SATI instrument at the tropical station Pune from October 2012 to December 2014. In this paper preliminary results from SATI observations are shown for 10 December 2012 and 3 March 2013 as an example of solstice and equinox. We employ the WACCM model to study the tidal characteristic during solstice and equinox. The variations in SATI observed emission rates and temperature with respect to WACCM simulations on individual nights may be related to the variability of tides. WACCM simulations show a dominant semidiurnal tide during solstice and a diurnal tide during equinox. The conclusions may be summarized as follows.

1. Both SATI OH temperature and WACCM temperature at 87 km, on 10 December 2012, show maxima at 2 hours before midnight and SATI O_2 temperature and WACCM temperature at 95 km show maxima at 3-4 hours before midnight. The maximum in O_2 temperature is higher (by ~30K) than OH temperature indicating that the O_2 emission is above the mesopause.

2. WACCM simulations show existence of both semidiurnal and diurnal tides during equinox and solstice. During equinox, the amplitude of the diurnal tide is stronger than the semidiurnal tide (at 87 km). The SATI OH temperature on 3 March 2013 (Equinox) indicates the existence of a semidiurnal tide and there is no prevalence of diurnal tide which is predicted by the WACCM model. The existence of a semidiurnal tide during equinox is also observed in the ground-based measurements by Friedman et al., (2009) who reported the existence of semidiurnal tides during all the seasons for the same

latitude. It is also consistent with the satellite results from SABER that showed a minimum in diurnal tide amplitude at 20° latitude (Mukhtarov et al., 2009).

3. During solstice, on 10 December 2012, the amplitude of the semidiurnal tide in SATI OH temperature is 25K and in WACCM (at 87km) it is ~10 K and the estimated amplitude from WACCM simulations for the complete solstice period is ~3.8K. For O_2 it is ~27K for SATI and ~9.8 K for WACCM (at 96 km) and from WACCM simulated for the complete solstice period it is ~4.8K. This indicates that the amplitude of semidiurnal tides is larger than estimated by WACCM for these days, and possibly all days. The SWM-95 model also underestimated diurnal tides (Hagan et al., 1999; Forbes and Wu., 2006).

4. The analysis of correlation between OH/O_2 emission rates and corresponding temperature (both SATI observations and WACCM simulations) shows positive correlation on 10 December 2012 (solstice) and 3 March 2013 (equinox). Although SATI data are sparse during equinox a positive correlation persists. This shows that lower/higher temperature corresponds to lower/higher emission rates indicating vertical motions and the dominance of dynamics over chemistry. A similar positive correlation is also reported by Cho and Shepherd (2006) at a high latitude station, Resolute Bay (74.68 ^{O}N). Therefore this paper shows that the positive correlation is general, not limited to one particular region.

5. The calculated atomic oxygen fluxes corresponding to vertical advection exhibit a variation that is semidiurnal during solstice and diurnal during equinox, suggesting that vertical advection associated with tides dominates the transport of atomic oxygen.

Acknowledgements: The modeling work at the University of Leeds is funded by the European Research Council (project number 291332 - CODITA). We thank anonymous reviewers for valuable suggestions.

References

Akmaev R. A., 2001; Seasonal variations of the terdiurnal tide in the mesosphere and lower thermosphere: A model study, Geophy. Res., Lett., 28, 19, 3817-3820, 2001.

Angelats i Coll, M., and Forbes, J. M., 1998. Dynamical influences on atomic oxygen and 5577 A emission rates in the lower thermosphere, Geophys. Res. Lett., 25(4), 461 – 464.

Beig, G., Fadnavis, S., Schmidt, H., and Brasseur, G. P., 2012. Inter-comparison of 11-year solar cycle response in mesospheric ozone and temperature obtained by HALOE satellite data and HAMMONIA model, J. Geophys. Res., 117, D00P10, doi:10.1029/2011JD015697.

Chamberlain, J. W., 1961. Physics of the aurora and airglow, Int. Geophys. Ser., vol. 2, Elsevier, Academic Press, New York.

Chang, L.C., Ward, W.E., Palo, S.E., Du, J., Wang, D.-Y., Liu, H.-L., Hagan, M.E., Portnyagin, Y., Oberheide, J., Goncharenko L.P., Nakamura, T., Hoffmann, P., Singer, W., Batista, P., Clemesha, B., Manson A.H., Riggin D.M., She, C.-Y., Tsuda, T., Yuan, T., 2012. Comparison of diurnal tide in models and ground-based observations during the 2005 equinox CAWSES tidal campaign, J. Atmos. Sol. Terr. Phys., 78–79, 19–30, doi:10.1016/j.jastp.2010.12.010.

Cho, Y.-M., and Shepherd, G. G., 2006. Correlation of airglow temperature and emission rate at Resolute Bay (74.68 ^{O}N), over four winters (2001–2005), Geophys. Res. Lett., 33, L06815, doi:10.1029/2005GL025298.

Crary, D. J., and J. M. Forbes, 1983. On the extraction of tidal information from measurements covering a fraction of a day, Geophys. Res. Lett., 10(7), 580-582.

Espy P. J., Stegman J., Forkman P., Murtagh D., 2007. Seasonal variation in the correlation of airglow temperature and emission rate, Geophys. Res. Lett. 34, 17, L17802, DOI: 10.1029/2007GL031034

Feng, W., Höffner, J., Marsh, D. R., Chipperfield, M. P., Dawkins, E. C. M., Viehl, T. P. and Plane, J. M. C., 2015. Diurnal variation of the potassium layer in the upper atmosphere, Geophys. Res. Lett., 42, 3619-3626, doi:10.1002/2015GL063718.

Feng, W., Marsh, D. R., Chipperfield, M. P., Janches, D., Höffner, J., Yi F., and Plane, J. M. C., 2013. A global atmospheric model of meteoric iron, J. Geophys. Res. Atmos., 118, 9456–9474, doi:10.1002/jgrd.50708.

Forbes, J., M. and Wu D., 2006, Solar Tides as Revealed by Measurements of Mesosphere Temperature by the MLS Experiment on UARS, J. Atmos, Sci., 63, 1776-1797.

Forbes, J. M., Roble R. G., and Fesen C. G., 1993. Acceleration, heating and compositional mixing of the thermosphere due to upward propagating tides, J. Geophys. Res., 98, 311 – 321.

Friedman, J. S., Zhang, X., Chu, X. and Forbes, J. M., 2009. Longitudinal variations of the solar semidiurnal tides in the mesosphere and lower thermosphere at low latitudes observed from ground and space, J. Geophys. Res., 114, D11,114, doi: 10.1029/2009JD011763.

Friedman, J. S. and Chu, X., 2007. Nocturnal temperature structure in the mesopause region over the Arecibo Observatory (18.35◦N,66.75◦W): Seasonal variations, J. Geophys. Res., 112, D14,107, doi:10.1029/2006JD008220

Ghodpage, R. N., Taori, A., Patil, P. T., Siingh, D., Gurubaran, S. and Sharma, A. K., 2015. On the vertical wavelength estimates using the Krassovsky parameters of OH airglow monitoring, Curr. Sci, 108, NO. 7.

Ghodpage, R. N., Siingh Devendraa, Singh R. P., Mukherjee, G. K., Vohat, P., and Singh, A K., 2012. Tidal and gravity waves study from the airglow measurements at Kolhapur (India), J. Earth Syst. Sci. 121, No. 6, 1511–1525.

Gogawale, A.D. and Tillu, S.R., 1983. Intensity variations and ratios of (9-4) and (7-3) hydroxyl bands in nightglow at Poona, Planetary and Space Science, 31, 423–433.

Guharay, A., Nath, D., Pant, P., Pande, B., Russell III, J. M., and Pandey, K., 2009. Observation of semiannual and annual oscillation in equatorial middle atmospheric long term temperature pattern, Ann. Geophys., 27, 4273–4280.

Gurubaran, S., Rajaram, R., Nakamura, T., Tsuda, T., Riggin, D., and Vincent, R. A., 2009. Radar observations of the diurnal tide in the tropical mesosphere-lower thermosphere region: Longitudinal variabilities, Earth Planets Space, 61, 513–524.

Gurubaran, S., Rajaram, R., Nakamura, T., and Tsuda, T., 2005. Interannual variability of diurnal tide in the tropical mesopause region: A signature of the El Nino-Southern Oscillation (ENSO), Geophys. Res. Lett., 32, L13805, doi:10.1029/2005GL022928.

Hagan, M. E., 2000. Modeling atmospheric tidal propagation across the stratopause, in atmospheric Science across the stratopause, Geophys. Monogr. Ser., vol. 123, edited by D. E. Siskind, S. D. Eckermann, and M. E. Summers, pp. 177 – 190, AGU, Washington, D. C.

Hagan, M. E., Burrage, M.D., Forbes, J., M., Hackney., J., Randel, W. J., and Zhang, X., 1999. GSWM-98: Results for migrating solar tides, J. Geophy., Res, 104, 6813-6827.

Hagan, M. E., McLandress, C., and Forbes, J. M. 1997. Diurnal tidal variability in the upper mesosphere and lower thermosphere, Annales Geophysicae ,15, 9, pp. 1176-1186).

Hernandez, G., Wiens, R. P. Lowe, Shepherd, G. G., Fraser, G. J., Smith, R. W., LeBlanc, L. M., and Clark, M.,1995. Optical determination of the vertical wavelength of propagating 12-hour period upper atmosphere oscillations, Geophys. Res. Lett. 22, 2389-2392.

Hays, P. B., Wu, D. L., Burrage, M.D., Gell, D. A, Grassl, H. J., Lieberman, R. S., Marshall, A. R., Morton, Y. T., Ortland, D. A., and Skinner, W. R., 1994. Observations of the diurnal tide from space, J. Atmos. Sci., 51, 3077-3093.

Hecht, J.H., Kane, T.J., Walterscheid, R.L., Gardner, C.S., Tepley, C.A. 1993. Simultaneous nightglow and Na lidar observations at Arecibo during the AIDA-89 campaign, J. Atmos. Terr. Phys., 55, 409-423.

(https://www.cs.cmu.edu/afs/andrew/scs/cs/15463/2001/pub/www/notes/fourier/fourier.pdf)

Hibbins, R. E., Freeman, M. P. , Milan, S. E. , and Ruohoniemi, J. M., 2011. Winds and tides in the mid-latitude Southern Hemisphere upper mesosphere recorded with the Falkland Islands SuperDARN radar, Ann. Geophys., 29, 1985-1996, doi:10.5194/angeo-29-1985-2011

Jaya Prakash Raju, U., Keckhut, P., Courcoux Y., Marchand, M., Bekki, S., Morel, B., Bencherif, H., Hauchecorne, A., 2010. Nocturnal temperature changes over tropics during CAWSES-III campaign: Comparison with numerical models and satellite data, J., Atmos., Terr., Phys., 72, 1171-1179.

Joan A., Propagation of Mountain Waves Into the Mesosphere as Observed by Satellite, 37th COSPAR Scientific Assembly. Held 13-20 July 2008, in Montréal, Canada., p.53, 2008.

Kishore Kumar, G., Singer, W., Oberheide, J., Grieger, N. , Batista, P.P., Riggin, D.M., Schmidt, H. , Clemesha, B.R., 2014. Diurnal tides at low latitudes: Radar, satellite, and model results, Journal of Atmospheric and Solar-Terrestrial Physics 118, 96–105.

Kishore Kumar, G., Venkat Ratnam, M., Patra, A. K., Vijaya, Bhaskara Rao, S., Russell J., 2008. Mean thermal structure of the low-latitude middle atmosphere studied using Gadanki Rayleigh lidar, Rocket, and SABER/TIMED observations. J. Geophys. Res. 113:D23106,doi:10.1029/2008JD010511.

Lieberman, R. S., Riggin, D. M., Ortland, D. A., Nesbitt, S. W., and Vincent, R. A., 2007. Variability of mesospheric diurnal tides and tropospheric diurnal heating during 1997–1998, J. Geophys. Res., 112, D20110, doi:10.1029/2007JD008578.

Liu, H.-L., Yudin, V. A. and Roble, R. G., 2013. Day-to-day ionospheric variability due to lower atmosphere perturbations, Geophys. Res. Lett., 40, 665–670, doi:10.1002/grl.50125.

Liu, G., Shepherd, G. G., and Roble, R. G., 2008. Seasonal variations of the nighttime O(1S) and OH airglow emission rates at mid-to-high latitudes in the context of the large-scale circulation, J. Geophys. Res., 113, A06302, doi:10.1029/2007JA012854.

Liu, H., and Roble, R.G., 2004: Dynamical processes related to the atomic oxygen equinox transition. Journal of Atmospheric and Solar-Terrestrial Physics, **66**, 769-779, DOI: 10.1016/j.jastp.2004.01.024.

López-González, M. J., García-Comas, M., Rodríguez, E., López-Puertas, M., Shepherd, M. G., Shepherd, G. G., Sargoytchev, S., Aushev, V. M., Smith, S. M., Mlynczak, M. G., Russell, J. M., Brown, S., Cho, Y.-M., Wiens, R.H., 2007.Ground-based mesospheric temperatures at mid-latitude derived from O_2 and OH airglow SATI data: Comparison with SABER measurements, Atmos. Solar-Terr. Phys., 69, 2379–2390.

López-González, M. J., Rodríguez, E., Shepherd, G. G., Sargoytchev, S., Shepherd, M. G., Aushev, V. M., Brown, S., García-Comas, M., and Wiens, R. H., 2005. Tidal variations of O_2 Atmospheric and OH (6-2) airglow and temperature at mid-latitudes from SATI observations, Ann. Geophy., 23, 3579–3590, SRef-ID: 1432-0576/ag/2005-23-3579.

López-González, M. J., Rodríguez, E., Wiens, R. H., Shepherd, G. G., Sargoytchev, S., Brown, S., Shepherd, M. G., Aushev, V. M., Lopez-Moreno, J. J., Rodrigo, R., and Cho, Y.-M., 2004. Seasonal variations of O2 atmospheric and OH(6–2) airglow and temperature at mid-latitudes from SATI observations, Ann, Geophys., 22, 819–828.

Manson, A. H., Meek, C. E., Luo, Y., Hocking, W. K., MacDougall, J., Riggin, D., Fritts, D. C., and Vincent, R. A., 2003. Modulation of gravity waves by planetary waves (2 and 16 d): observations with the north American-Pacific MLT-MFR radar network, J. Atmos. Sol. Terr. Phys., 65(1), 85-104.

Manson, A. H., Meek, C. E., and Hall, G. E., 1998. Correlations of gravity waves and tides in the mesosphere over Saskatoon, J. Atmos. Sol. Terr. Phys., 60, 1089–1107.

Marsh, D., Janches, D., Feng, W., and Plane, J. M. C., 2013. A global model of meteoric sodium, J. Geophys. Res. Atmos., 118, 11,442–11,452, doi:10.1002/jgrd.50870.

Marsh, D. R., Smith, A. K., Mlynczak, M. G., and Russell III, J. M., 2006. SABER observations of the OH Meinel airglow variability near the mesopause, J. Geophy. Res., 111, A10S05, doi:10.1029/2005JA011451.

Marsh, D. R., and Russell III, J. M., 2000. A tidal explanation for the sunrise/ sunset anomaly in HALOE low-latitude nitric oxide observations, Geophys. Res. Lett., 27, 3197 – 3200.

McDade, I. C., and Llewellyn, E. J. (1986), The excitation of O (^{1}S) and O_2 bands in the nightglow: A brief review and preview, Can. J. Phys., **64**, 1626–1630.

McLandress, C., 2002. The seasonal variation of the propagating diurnal tide in the mesosphere and lower thermosphere. Part II: The role of tidal heating and zonal mean winds, J. Atmos. Sci., 59(5), 907 – 922.

McLandress, C., Shepherd, G. G., and Solheim, B. H., 1996. Satellite observations of thermospheric tides: Results from the Wind Imaging Interferometer on UARS, J. Geophys. Res., 101, 4093-4114.

Miyahara, S., Yoshida Y., and Miyoshi Y., 1993. Dynamic coupling between the lower and upper atmosphere by tides and gravity waves, J. Atmos. Terr. Phys., 55, 1039–1053.

Mukhtarov, P., D. Pancheva, and B. Andonov (2009), Global structure and seasonal and interannual variability of the migrating diurnal tide seen in the SABER/TIMED temperatures between 20 and 120 km, J. Geophys. Res., 114, A02309, doi:10.1029/2008JA013759.

Pant, T. K., D. Tiwari, C. Vineeth, S. V. Thampi, S. Sridharan, C. V. Devasia, R. Sridharan, S. Gurubaran, and R. Sekar, 2007. Investigation on the mesopause energetics and its possible implications on the equatorial MLTI processes through coordinated daytime airglow and radar measurements, Geophys. Res. Lett., 34, L15102, doi:10.1029/2007GL030193.

Pant, T. K., Tiwari, D., Sridharan, S., Sridharan, R., Gurubaran, S., Subbarao, K. S. V., and Sekar, R., 2004. Evidence for direct solar control of the mesopause dynamics through dayglow and radar measurements, Ann. Geophys., 22, 3299–3303.

Plane, J. M. C., Feng, W., Dawkins, E., Chipperfield, M. P., Höffner, J., Janches, D., and Marsh, D. R., 2014. Resolving the strange behavior of extraterrestrial potassium in the upper atmosphere, Geophys. Res. Lett., 41, 4753–4760, doi:10.1002/2014GL060334.

Ranade, N., Choudhary, P B. and Tillu, A. D., 1988. 5577 and 5893 emissions in the lower thermosphere and their dynamic coupling, Phys. Scr. 37, 496, doi:10.1088/0031-8949/37/3/037.

Sander, S. P., Friedl, R. R., Golden, D. M., Kurylo, M. J., Moortgat, G. K., Keller-Rudek, H., Wine, P. H., Ravishankara, A. R., Kolb, C. E., Molina, M. J., Finlayson-Pitts, B. J., Huie, R. E., and Orkin, V. L., 2006. Chemical kinetics and photochemical data for use in atmospheric studies, evaluation number 15, JPL publication 06-2, Jet Propulsion Laboratory, Pasadena, CA,

Sargoytchev, S., S. Brown, Solheim B. H., Cho Y.-M., Shepherd G. G., and López-González M. J., 2004. Spectral airglow temperature imager (SATI)—A ground based instrument for temperature monitoring of the mesosphere region, Appl. Opt., 43(30), 5712 – 5721.

Schubert, G., Walterscheid, R. L., Hickey, M. P. and Tepley, C. A. 1999. Observations of gravity wave induced fluctuations in the O I (557.7 nm) airglow, J. Geophys. Res., 104, A7, 14,915-14,924.

Shepherd, G.G., Thuillier, G., Cho, Y.-M., Duboin, M.-L., Evans, W.F.J., Gault, W.A., Hersom, C., Kendall, D.J.W., Lathuillère, C., Lowe, R.P., McDade, I.C., Rochon, Y.J., Shepherd, M.G., Solheim, B.H., Wang, D.-Y., and Ward, W.E., 2012. The Wind Imaging Interferometer (WINDII) on the Upper Atmosphere Research Satellite: A 20 year perspective. Rev. Geophys. 50, RG2007, doi:10.1029/2012RG000390.

Shepherd G. G., Roble R. G, Zhang S.-P., McLandress C., Wiens R. H., 1998. Tidal influence on midlatitude airglow: Comparison of satellite and ground-based observations with TIME-GCM predictions, J. Geophy. Res., 103,A7, 14741–14751, DOI: 10.1029/98JA00884.

Shepherd, G. G., McLandress, C., and Solheim, B. H., 1995. Tidal influence on $O(^1S)$ airglow emission rate distributions at the geographic equator as observed by WINDII, Geophys. Res. Lett., 22, 275-278.

Smith, A.K., 2012. Global dynamics of the MLT. Surv. Geophys. 33 (6), 1177–1230.

Smith, A. K., Marsh D. R., and Szymczak A. C., 2003. Interaction of chemical heating and the diurnal tide in the mesosphere, J. Geophys. Res., 108(D5), 4164, doi:10.1029/2002JD002664.

Takahashi, H., Onohara, A., Shiokawa, K., Vargas, F., and Gobbi, D., 2011, Atmospheric wave induced O2 and OH airglow intensity variations: effect of vertical wavelength and damping, Ann. Geophys., 29, 631–637, 2011, doi:10.5194/angeo-29-631-2011.

Takahashi, H., Nakamura, T., Shiokawa, K., Tsuda, T., Lima, L. M., and Gobbi, D., 2004. Atmospheric density and pressure inferred from the meteor diffusion coefficient and airglow O2b temperature in the MLT region, Earth Planets Space, 56, 249–258.

Taori, A., Jayaraman, A., Raghunath, K., and Kamalakar, V., 2012. A new method to derive middle atmospheric temperature profiles using a combination of Rayleigh lidar and O2 airglow temperatures measurements, Ann. Geophys., 30, 27–32, doi:10.5194/angeo-30-27-2012.

Taori, A., Makela, J. J., and Taylor, M., 2010. Mesospheric wave signatures and equatorial plasma bubbles: A case study, J. Geophys. Res., 115, A06302, doi:10.1029/2009JA015088.

Taori, A., Guharay, A., and Taylor, M. J., 2007. On the use of simultaneous measurements of OH and O2 emissions to investigate wave growth and dissipation, Ann. Geophys., 25, 639–643.

Taori, A. and M. Taylor, 2006. Characteristics of wave induced oscillations in mesospheric O2 emission intensity and temperatures, Geophys. Res. Lett., 33, L01813, doi:10.1029/2005GL024442.

Taori, A., Taylor, M. J., and Franke, S., 2005. Terdiurnal wave signatures in the upper mesospheric temperature and their association with the wind fields at low latitudes (20◦N), J. Geophys. Res., 110, D09S06, doi:10.1029/2004JD004564, 2005.

Vargas, F., Swenson, G., Liu, A. Z. and Gobbi, D., 2007. O(1 S), OH, and O2(b) airglow layer perturbations due to AGWs and their implied effects on the atmosphere, J. Geophys. Res., 112, D14102, doi:10.1029/2006JD007642.

Walterscheid, R. L., Hecht, J. H., Djuth, F. T. and Tepley, C. A., 2000. Evidence of a long-period gravity wave in observations of the nightglow over Arecibo on May 8-9, 1989, J. Geophys. Res., 105, D5, 6927-6934.

Ward, W. E., Oberheide, J., Riese, M., Preusse, P., and Offermann, D., 1999. Tidal signatures in temperature data from CRISTA 1 mission, J. Geophys. Res., 104(D13), 16,391 – 16,403.

Ward, W. E., 1999. A simple model of diurnal variations in the mesospheric oxygen nightglow, Geophys. Res. Lett., 26(23), 3565 – 3568.

Yuan, T., Schmidt, H., She, C.-Y., Krueger, D. A., and Reising, S., 2008a. Seasonal variations of semidiurnal tidal perturbations in mesopause region temperature and zonal and meridional winds above Fort Collins, Colorado (40.6°N, 105.1°W), J. Geophys. Res., 113, D20103, doi:10.1029/2007JD009687.

Yuan, T., She, C.-Y., Krueger, D. A., Sassi, F., Garcia, R., Roble, R. G., Liu, H.-L., and Schmidt, H., 2008b. Climatology of mesopause region temperature, zonal wind, and meridional wind over Fort Collins, Colorado (41°N, 105°W), and comparison with model simulations, J. Geophys. Res., 113, D03105, doi:10.1029/2007JD008697.

Zeng, Z., Randel, W., Sokolovskiy, S., Deser, C., Kuo, Y.-H., Hagan, M., Du, J., and Ward, W., 2008. Detection of migrating diurnal tide in the tropical upper troposphere and lower stratosphere using the challenging minisatellite payload radio occultation data, J. Geophys. Res., 113, D03102, doi:10.1029/2007JD008725.

Zhang, X., Forbes, J. M., and Hagan, M. E., 2010. Longitudinal variation of tides in the MLT region: 1. Tides driven by tropospheric net radiative heating, J. Geophys. Res., 115, A06316, doi:10.1029/2009JA014897.

Zhang, S. P., Roble, R. G., and Shepherd, G. G. 2001. Tidal influence on the oxygen and hydroxyl nightglows: Wind Imaging Interferometer observations and thermosphere-ionosphere-mesosphere-electrodynamics general circulation model, J. Geophys. Res., 106, 21,381 – 21,393.

Zhou, Q. H., Monroy, H., Fritts, D. C., Ierkic, H. M., Isham, B., Isler, J. R., Palo, S. E., 2000. Radar observations of longitudinal variability of tidal/planetary waves and mean motions in the tropical mesosphere, J. Geophys. Res., 105, D2, 2151-2161, 27., 10.1029/1999JD901083

Zhu, X., Yee, J.-H., Strobel, D. F., Wang, X. and Greenwald, R. A. 1999. On the numerical modelling of middle atmosphere tides. Q.J.R. Meteorol. Soc., 125: 1825–1857. doi: 10.1002/qj.49712555717.

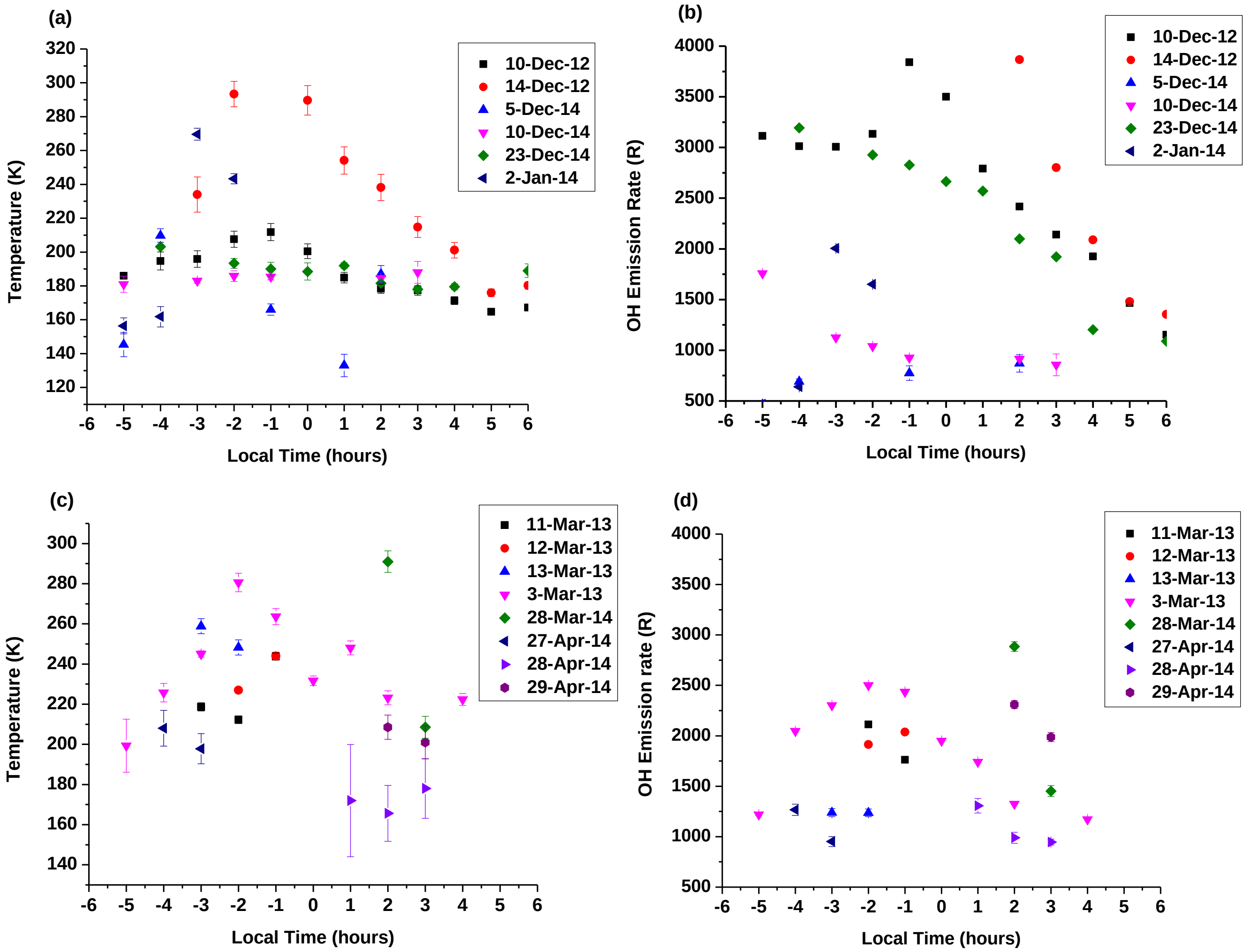

Figure 1: Hourly values versus time for (a) OH temperature during solstice (December-January) (b) OH emission rate in Rayleigh (R) at solstice (December-January) (c) OH temperature during equinox (March April) (d) OH emission rate in Rayleigh (R) during equinox (March April).

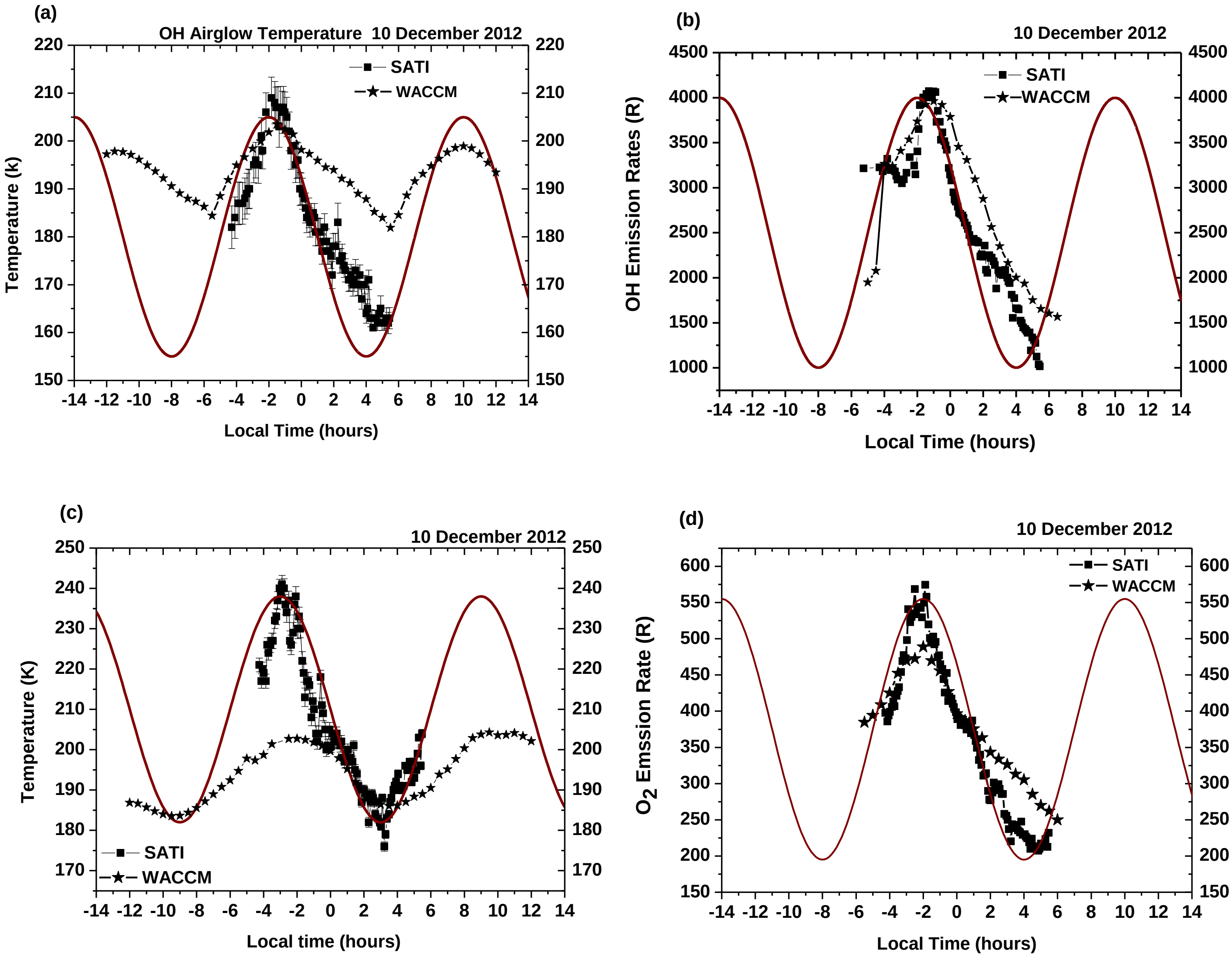

Figure 2: Variation of (a) OH temperature (b) OH emission rate in Rayleigh (R) (c) O_2 temperature (d) O_2 emission rates on 10 December 2012 as observed by SATI. The WACCM simulated temperature at 87 km are compared with OH temperature and at 95 km with O_2 temperature. Simulated OH and O_2 emission rates are compared with SATI observations in figures (b) and (d). Red curves show simulated sinusoidal waveform.

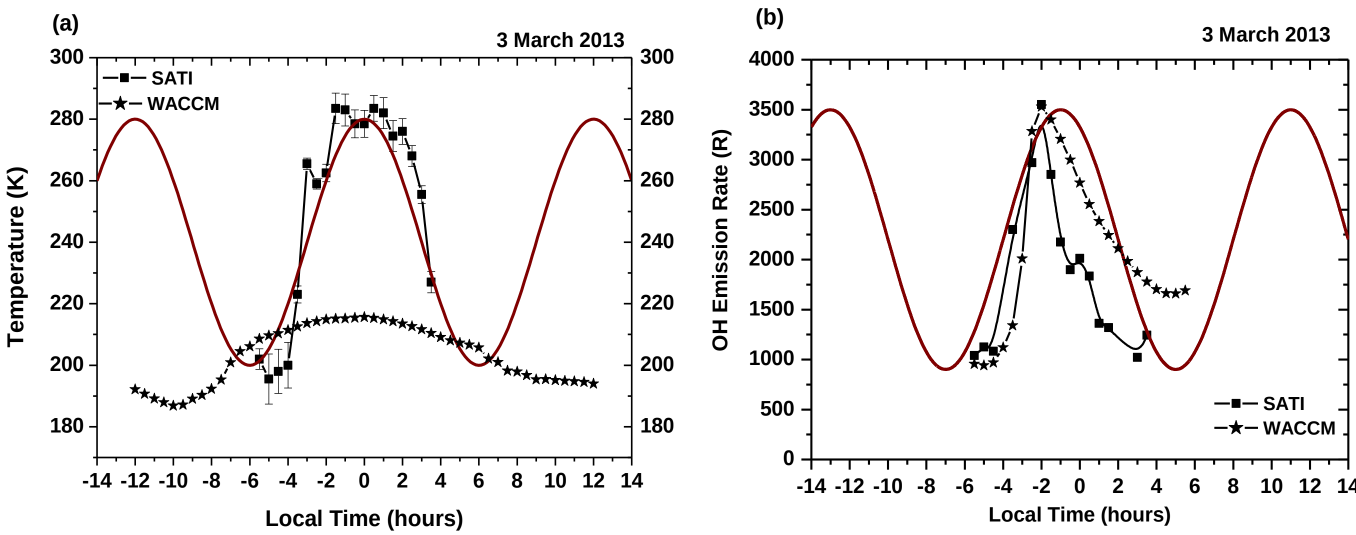

Figure 3: Variation of (a) OH temperature (b) OH emission rated in Rayleigh (R) as observed by SATI. The WACCM simulated temperature at 87 km and emission rate are compared with SATI observations. Red curves show simulated sinusoidal waveform.

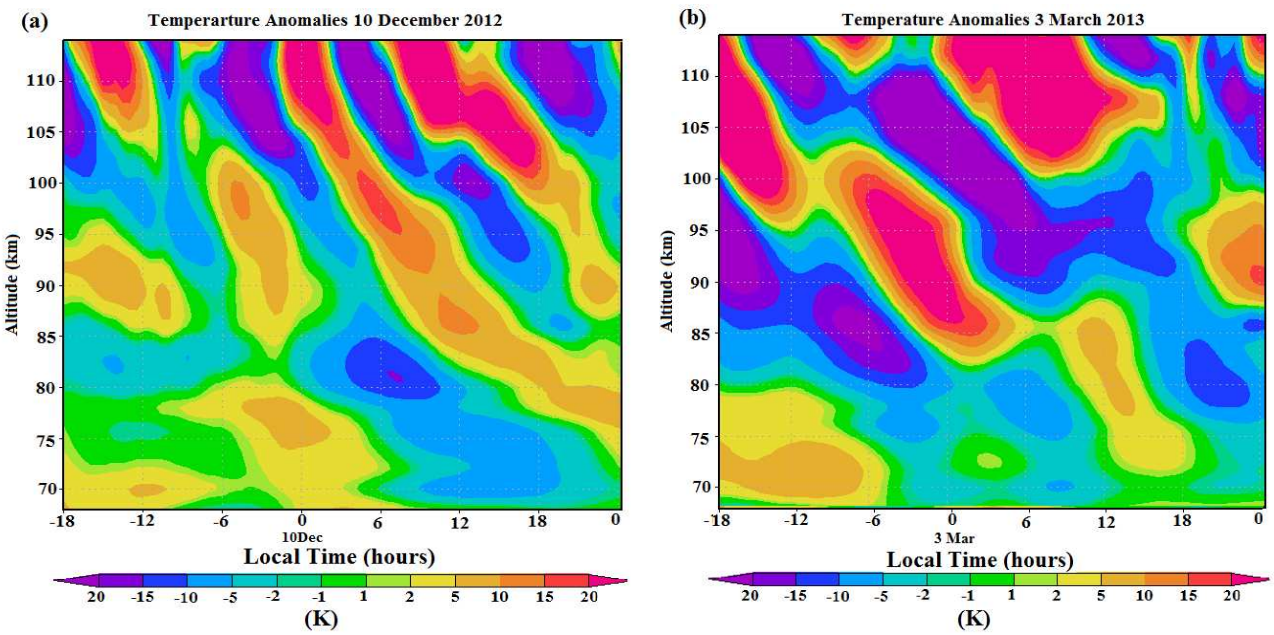

Figure 4: WACCM simulated vertical profiles of temperature anomalies (K) at Pune for (a) 10 December 2012 (b) 3 March 2013.

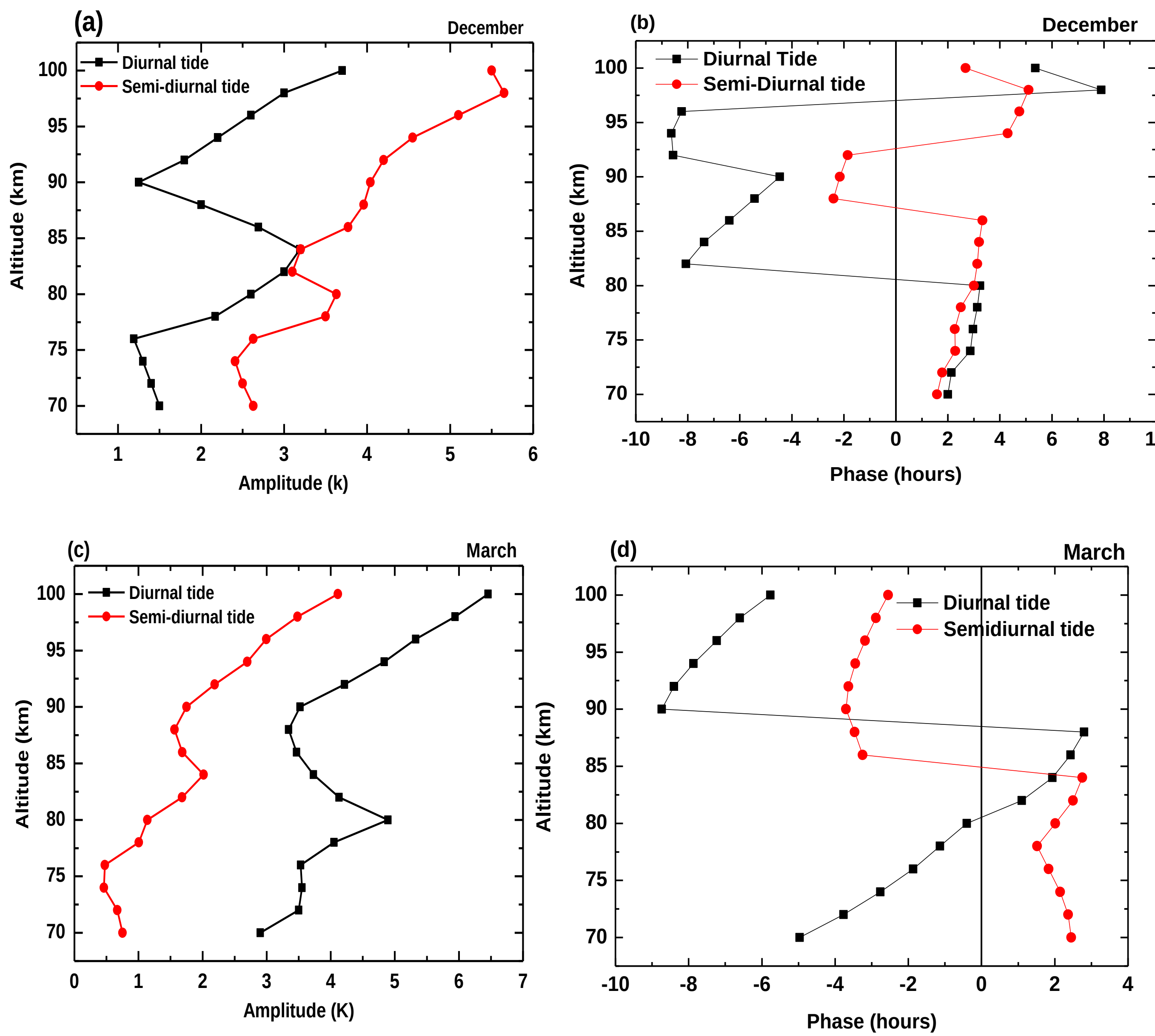

Figure 5: Vertical profiles of amplitude and phase of diurnal (black profile) and semi-diurnal (red profile) in temperature as obtained from WACCM simulations (a) amplitude (K) for December 2012 and 2013 (b) phase (hours) averaged for December 2012 and 2013. (c) and (d) same as (a) and (b) but for March 2012 and 2013.

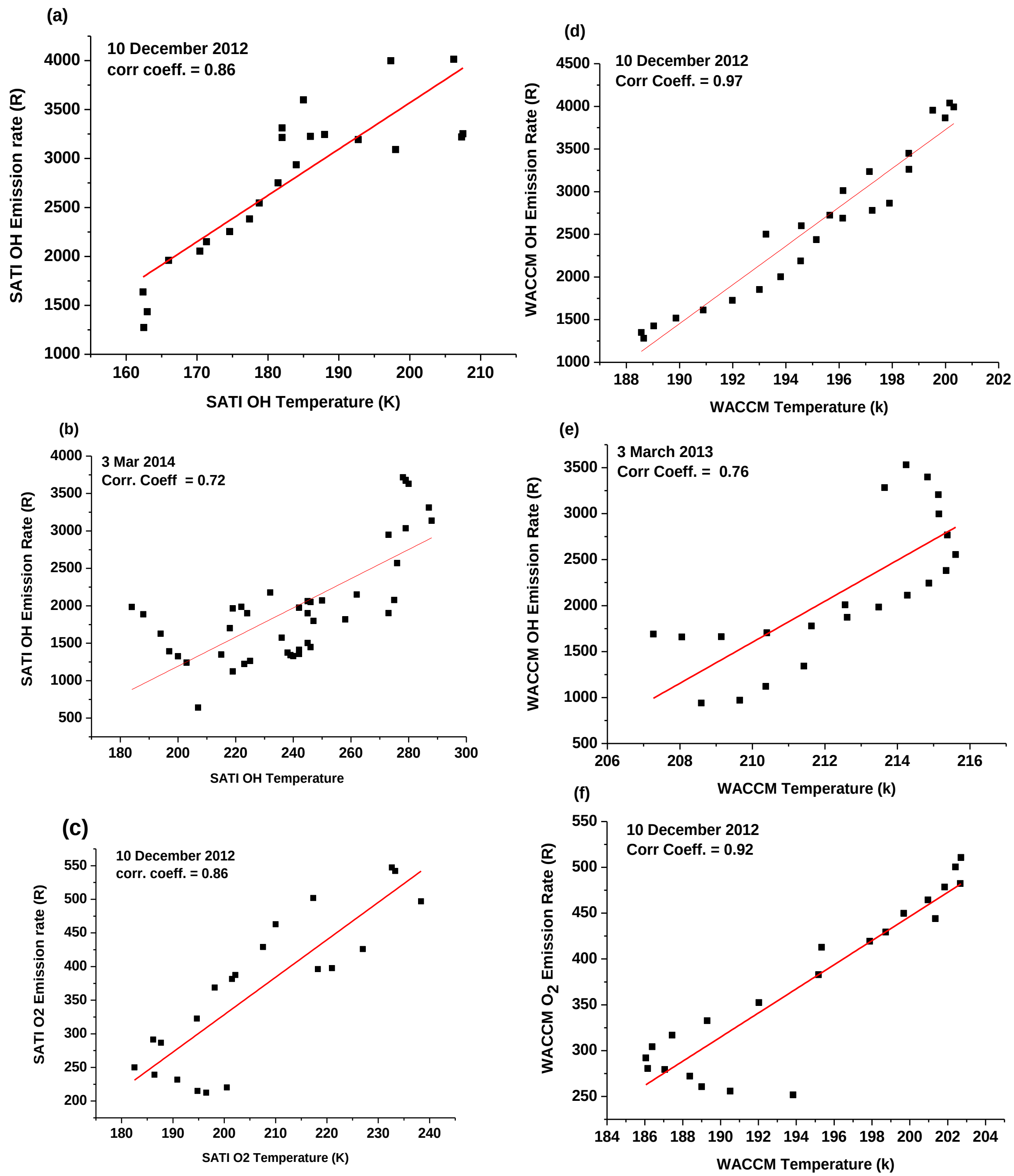

Figure 6: Scatter plots of the 30 minute averaged SATI data (a) temperature and emission rate in Rayleigh (R) of OH for 10 December 2012 (b) temperature and emission rate of OH in Rayleigh (R) for 3March 2012 (c) temperature and emission rate in Rayleigh (R) of O_2 for 10 December 2012. Figures (d)-(f), same as figures (a)-(c), but obtained from WACCM simulations. The solid lines are linear fits to the data.

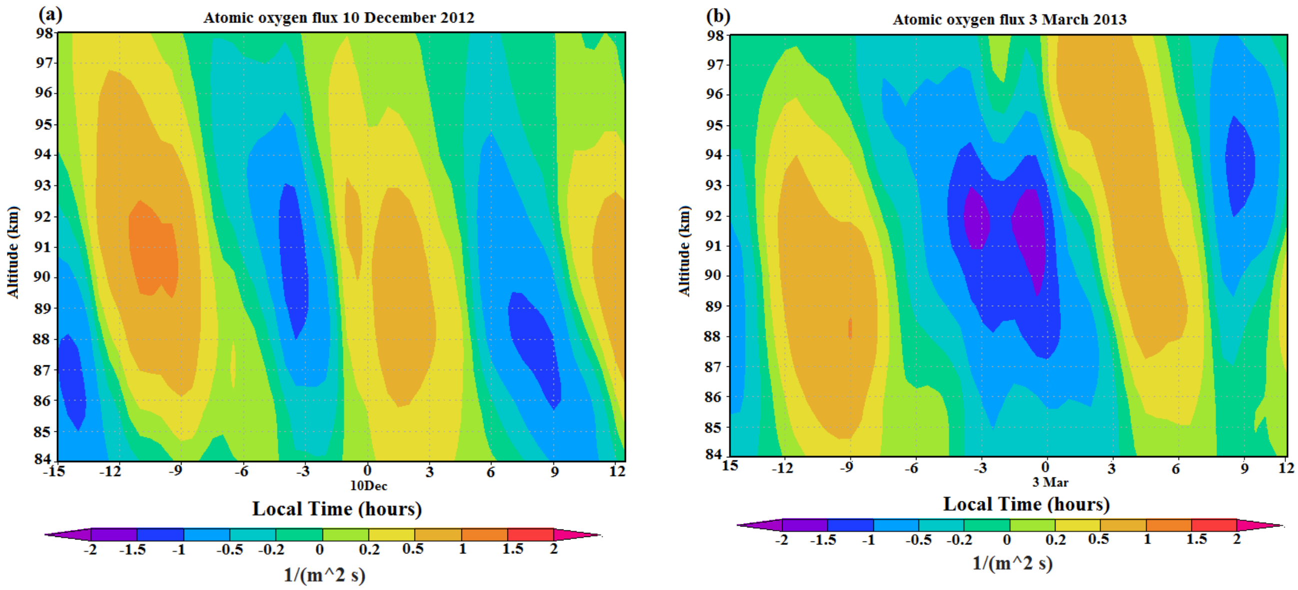

Figure 7: WACCM simulated vertical profiles of atomic oxygen flux (1/(m^2 s)) at Pune (a) 10 December 2012 (b) 3 March 2013. Positive anomalies indicate upward and negative anomalies downward motion.